



The Pulsating White Dwarf G117-B15A: Still the Most Stable Optical Clock Known

S. O. Kepler¹ , D. E. Winget² , Zachary P. Vanderbosch² , Barbara Garcia Castanheira³ , J. J. Hermes⁴ , Keaton J. Bell^{5,13} , Fergal Mullally⁶, Alejandra D. Romero¹ , M. H. Montgomery² , Steven DeGennaro^{2,14}, Karen I. Winget², Dean Chandler⁷, Elizabeth J. Jeffery⁸, Jamile K. Fritzen¹, Kurtis A. Williams⁹ , Paul Chote¹⁰, and Staszek Zola^{11,12}

¹ Instituto de Física, Universidade Federal do Rio Grande do Sul, 91501-970 Porto Alegre RS, Brazil; kepler@if.ufrgs.br

² Department of Astronomy and McDonald Observatory, University of Texas at Austin, Austin, TX 78712-1085, USA

³ Baylor University, Department of Physics, Waco, TX 76798, USA

⁴ Department of Astronomy, Boston University, Boston, MA 02215, USA

⁵ DIRAC Institute, Department of Astronomy, University of Washington, Seattle, WA 98195-1580, USA

⁶ SETI Institute, 189 Bernardo Avenue, Suite 200, Mountain View, CA 94043, USA

⁷ Meyer Observatory and Central Texas Astronomical Society, 209 Paintbrush, Waco, TX 76705, USA; chandler@vvm.com

⁸ Physics Department, California Polytechnic State University, San Luis Obispo, CA 93407, USA; elizabeth.j.jeffery@gmail.com

⁹ Department of Physics and Astronomy, Texas A&M University-Commerce, P.O. Box 3011, Commerce, TX 75429-3011, USA

¹⁰ Department of Physics, University of Warwick, Coventry CV4 7AL, UK; p.chote@warwick.ac.uk

¹¹ Astronomical Observatory of the Jagiellonian University, ul. Orla 171, PL-30-244 Kraków, Poland

¹² Mt. Suhora Observatory, Pedagogical University, ul. Podchorazych 2, PL-30-084 Kraków, Poland

Received 2020 September 28; revised 2020 October 26; accepted 2020 October 28; published 2020 December 29

Abstract

The pulsating hydrogen atmosphere white dwarf star G 117-B15A has been observed since 1974. Its main pulsation period at $215.19738823(63)$ s, observed in optical light curves, varies by only $(5.12 \pm 0.82) \times 10^{-15}$ s s $^{-1}$ and shows no glitches, as pulsars do. The observed rate of period change corresponds to a change of the pulsation period by 1 s in 6.2 million yr. We demonstrate that this exceptional optical clock can continue to put stringent limits on fundamental physics, such as constraints on interaction from hypothetical dark matter particles, as well as to search for the presence of external substellar companions.

Unified Astronomy Thesaurus concepts: White dwarf stars (1799); Late stellar evolution (911)

1. Introduction

G 117-B15A, also called RY LMi and WD 0921+354, is a pulsating white dwarf with a hydrogen atmosphere, a DAV or ZZ Ceti star (McGraw 1979). White dwarf stars are the most common end product of stellar evolution. From the observed initial-mass-function, more than 97% of all stars evolve to white dwarfs (Fontaine et al. 2001; Koester 2002; Smartt 2009; Althaus et al. 2010; Woosley & Heger 2015; Lauffer et al. 2018). When the normal white dwarf cooling reduces their temperatures such that the their outer envelopes develop partial ionization zones—which depends on the dominant chemical element in the envelope—convection zones are established that drive pulsations. These pulsations are seen as luminosity variations and the period of the dominant pulsation mode is related to the thermal timescale at the base of the envelope. These white dwarf stars show multiperiodic nonradial *g*-mode pulsations that—being global—can be used to measure their internal properties and their rate of evolution (Fontaine & Brassard 2008; Winget & Kepler 2008; Althaus et al. 2010; Vauclair 2013; Córscico et al. 2019).

McGraw & Robinson (1976) found G 117-B15A to be variable, and Kepler et al. (1982) found six simultaneous excited periods in its light curve. The dominant mode has a period of 215 s, a fractional optical amplitude around 22 mma (millimodulation amplitude, or parts per thousand), and is stable in amplitude and phase. The other, smaller pulsation modes, vary in amplitude from night to night (Kepler et al. 1995), either caused by internal instabilities or unresolved components. Because the DAVs are normal stars except for

their variability (Robinson 1979; Bergeron et al. 1995, 2004; Castanheira et al. 2013; Romero et al. 2013), i.e., an evolutionary stage in the cooling of all white dwarfs, it is likely that the DAV structural properties are representative of all hydrogen atmosphere—DA—white dwarfs. DA white dwarfs comprise more than 80% of all white dwarfs (e.g., Kepler et al. 2019).

In their review of the properties of pulsating white dwarfs, Córscico et al. (2019) list the 250 ZZ Cetis known at the time. Since then, 39 additional ZZ Cetis have been published (Vincent et al. 2020).

We report our continuing study of the star G 117-B15A, one of the hottest of the ZZ Ceti stars. The rate of change of a pulsation period with time for *g*-mode pulsations in white dwarf stars is theoretically directly related to its evolutionary timescale (Winget et al. 1983), allowing us to infer the age of a cool white dwarf. We have been observing the star since 1974 to measure the rate of period change with time (\dot{P}) for the largest amplitude periodicity, at 215 s. Using all the data obtained from 1974 through 2005, Kepler et al. (2005) estimated the intrinsic rate of period change

$$\dot{P}_i = \dot{P}_{\text{observed}} - \dot{P}_{\text{pm}} = (3.79 \pm 0.81) \times 10^{-15} \text{ s s}^{-1}.$$

The quoted uncertainty was the intrinsic one from the fit only.

Kepler (1984) demonstrated that the observed variations in the light curve of G 117-B15A are due to nonradial *g*-mode pulsations. Kepler et al. (2000) show that the models predict the effect of radius change due to the still ongoing contraction are an order of magnitude smaller than the cooling effect on the rate of period change.

Concerning the expected stability of pulsation modes, Hermes et al. (2017) used Kepler and K2 data to show that

¹³ NSF Astronomy and Astrophysics Postdoctoral Fellow.

¹⁴ IMDb.

modes with periods longer than about 800 s are considerably less coherent than shorter period modes, with their power spectra often having a “mottled” appearance. Montgomery et al. (2020) showed that this could be explained by the longer period modes having a stronger interaction with the surface convection zone of the star, since they have turning points much closer to the surface than low-period modes. We return to this question with regards to G 117–B15A in Section 5.1.2.

G 117–B15A is proving to be a useful laboratory for particle physics (Isern et al. 2004). Córscico et al. (2001) calculated the limit on the axion mass compatible with the then observed upper limit to the cooling, showing $m_a \cos \beta \leq 4.4$ meV and Kepler (2004) demonstrates axion cooling would be dominant over neutrino cooling for the lukewarm white dwarf stars for axion masses of this order. Biesiada & Malec (2002) show that the 2σ upper limit published in Kepler et al. (2000) limits the string mass scale $M_S \geq 14.3 \text{ TeV}/c^2$ for six dimensions, from the observed cooling rate and the emission of Kaluza–Klein gravitons, but the value is unconstrained for higher dimensions. Benvenuto et al. (2004) show the observed rates of period change can also be used to constrain the dynamical rate of change of the constant of gravity \dot{G} .

2. Observations

Kepler et al. (2005) reported on the observations from 1974 to 2005. In this paper we report on 178 hr of additional time series photometry from 2005 to 2020 (Table 1), most taken with the Argos prime-focus CCD camera (Nather & Mukadam 2004) on the 2.1 m Otto Struve telescope at McDonald Observatory.

We use the BG40 filter on all observations because it increases the contrast between the (mostly blue) pulsational amplitude and the (mostly red) sky background. Also, the sky background is variable, and introduces strong systematics. Nonradial g -mode light variations have the same phase in all colors (Robinson et al. 1982) but the amplitudes decrease with wavelength. For example, a filter-less observation with Argos gives an amplitude around 40% smaller for G 117–B15A.

3. Data Reduction

We reduce and analyze the data in the manner described by Nather et al. (1990) and Kepler (1993). We bring all the data to the same fractional amplitude scale, and the times from terrestrial UTC to the uniform Barycentric Julian Coordinated Date (TCB) scale, using JPL DE405 ephemeris (Standish 1998, 2004) to model Earth’s motion. We compute Fourier transforms for each individual run, and verify that the main pulsation at 215 s dominates each data set and has an amplitude stable up to 15%, our uncertainty in amplitude due to the lack of accurate time and color-dependent extinction determination.

4. Timescale for Period Change

As the dominant pulsation mode at $P = 215$ s has been stable in frequency and amplitude since our first observations in 1974, we can calculate the time of maximum for each new run and look for deviations from those assuming a constant period.

Table 1
Journal of Observations Since 2005

Date	Exposure (s)	Duration (s)	Number	Telescope
2005 Dec 5	5	7040	1408	McD 2.1 m
2005 Dec 9	5	12000	2400	McD 2.1 m
2006 Mar 1	5	14020	2804	McD 2.1 m
2006 Mar 4	5	9305	1861	McD 2.1 m
2006 Mar 6	10	13140	1314	McD 2.1 m
2006 Dec 21	10	4280	428	McD 2.1 m
2006 Dec 28	5	15730	3147	McD 2.1 m
2007 Mar 16	5	2865	545	McD 2.1 m
2007 Apr 10	5	6775	1355	McD 2.1 m
2008 Feb 9	5	16040	3208	McD 2.1 m
2008 Mar 11	5	10175	2035	McD 2.1 m
2008 Mar 13	5	9900	1980	McD 2.1 m
2008 Mar 14	5	3600	720	McD 2.1 m
2009 Jan 29	5	15035	3008	McD 2.1 m
2009 Jan 30	5	14400	2881	McD 2.1 m
2009 Feb 3	5	10315	2064	McD 2.1 m
2009 Apr 13	20	7400	370	0.6 m Suhora
2009 Apr 15	22	6974	317	0.6 m Suhora
2009 Apr 24	10	9030	903	McD 2.1 m
2010 Jan 10	5	3840	768	McD 2.1 m
2010 Jan 20	5	7320	1465	McD 2.1 m
2010 Feb 16	5	10805	2161	McD 2.1 m
2010 Feb 19	10	10740	1075	McD 0.9 m
2010 Mar 10	15	7380	493	McD 0.9 m
2010 Mar 11	15	18480	1233	McD 0.9 m
2010 Mar 17	10	18350	1836	McD 0.9 m
2010 Mar 18	10	27030	2704	McD 0.9 m
2010 Mar 19	10	22910	2292	McD 0.9 m
2010 Mar 21	15	20160	1345	McD 0.9 m
2010 Apr 10	10	14640	1464	McD 2.1 m
2010 Apr 16	10	1360	137	McD 2.1 m
2010 Dec 12	10	17530	1753	McD 2.1 m
2011 Jan 6	10	5810	581	McD 2.1 m
2011 Jan 9	10	9770	977	McD 2.1 m
2011 Feb 1	10	9870	987	McD 2.1 m
2013 Apr 13	5	7900	1580	McD 2.1 m
2013 Apr 23	5	10800	2160	McD 2.1 m
2013 Apr 25	5	12670	2534	McD 2.1 m
2015 Jan 17	30	30240	890	McD 2.1 m
2015 Jan 18	30	10620	344	McD 2.1 m
2015 Mar 14	10	11070	1101	McD 2.1 m
2015 Mar 16	20	18700	826	McD 2.1 m
2015 Mar 19	14	14266	1019	McD 2.1 m
2015 Mar 20	25	8100	294	McD 2.1 m
2018 Jan 26	15	15720	1049	McD 2.1 m
2018 Jan 27	5	14285	2856	McD 2.1 m
2018 Jan 28	10	12460	1247	McD 2.1 m
2018 Mar 12	10	5380	539	McD 2.1 m
2018 Mar 13	10	12480	742	McD 2.1 m
2018 Mar 14	10	9710	673	McD 2.1 m
2018 Mar 15a	10	4350	435	McD 2.1 m
2018 Mar 15b	10	1940	195	McD 2.1 m
2019 Jan 5	3	20142	6713	McD 2.1 m
2020 Feb 20	20	8400	380	McD 2.1 m
2020 Feb 23	15	18960	1132	McD 2.1 m

We fit our observed time of maximum light, O , given in Table 2, to the equation for the difference to the calculated one, C :

$$(O - C) = \Delta E_0 + \Delta P \cdot E + \frac{1}{2} P \cdot \dot{P} \cdot E^2,$$

Table 2
Total Data Set to Date

Time of Maximum BJDD	Epoch of Maximum	$O - C$ (s)	σ (s)
2442397.917507	0	0.0	2.1
2442477.797089	32071	0.5	1.7
2442779.887934	153358	3.9	2.1
2442783.850624	154949	1.2	2.9
2442786.981458	156206	2.2	1.5
2443462.962774	427607	1.6	1.4
2443463.946592	428002	0.5	1.4
2443465.969049	428814	0.5	1.6
2443489.909755	438426	0.2	1.5
2443492.898616	439626	0.9	1.6
2443521.927837	451281	0.1	1.3
2443552.752879	463657	0.8	1.4
2443576.725940	473282	-1.6	3.3
2443581.692438	475276	0.3	1.3
2443582.693698	475678	-0.2	1.3
2443583.697469	476081	1.0	1.3
2443584.733602	476497	0.8	1.4
2443604.659292	484497	1.3	1.5
2443605.752703	484936	0.4	1.4
2443611.693050	487321	0.6	1.3
2443613.658222	488110	0.7	1.6
2443636.674491	497351	8.8	3.4
2443839.956765	578967	5.8	3.0
2443841.976708	579778	3.7	3.5
2443842.980413	580181	-0.7	2.2
2443843.944332	580568	0.5	2.6
2443869.989703	591025	1.5	2.4
2443870.946182	591409	5.5	3.1
2443874.916339	593003	2.4	2.1
2443959.695117	627041	0.1	2.0
2443963.662836	628634	1.6	2.1
2443990.664641	639475	2.7	1.3
2444169.945954	711455	0.1	1.6
2444231.822666	736298	-0.7	2.9
2444232.818992	736698	3.0	1.6
2444293.833896	761195	0.3	1.8
2444637.776174	899285	5.8	1.9
2444641.624287	900830	2.8	1.1
2444992.789531	1041820	0.1	1.6
2444994.689956	1042583	1.2	1.2
2444996.744801	1043408	2.0	1.3
2444997.723649	1043801	1.9	1.2
2445021.716661	1053434	1.7	1.4
2445703.860004	1327309	1.9	1.7
2445734.642701	1339668	2.4	1.2
2445735.643972	1340070	2.8	1.3
2446113.763716	1491882	2.9	1.2
2446443.775386	1624379	2.8	1.1
2446468.630178	1634358	2.1	1.3
2446473.718679	1636401	0.3	1.6
2446523.620086	1656436	2.2	1.6
2446524.613917	1656835	5.5	2.5
2446768.855451	1754896	2.9	1.4
2446794.935676	1765367	2.5	2.1
2446796.928219	1766167	0.3	1.6
2446797.924535	1766567	3.1	1.3
2446798.903378	1766960	2.6	1.8
2446823.663537	1776901	3.1	1.9
2446825.651132	1777699	3.7	1.5
2447231.328096	1940575	3.7	1.9
2447231.612054	1940689	5.1	3.5
2447232.396626	1941004	5.0	1.6
2447232.623291	1941095	5.9	2.9

Table 2
(Continued)

Time of Maximum BJDD	Epoch of Maximum	$O - C$ (s)	σ (s)
2447233.343090	1941384	4.5	1.3
2447233.634506	1941501	4.7	2.3
2447234.319475	1941776	6.8	3.2
2447235.313250	1942175	5.2	1.4
2447235.607168	1942293	6.4	2.1
2447236.610922	1942696	6.2	1.6
2447589.375198	2084328	3.2	1.4
2447594.331735	2086318	5.2	1.6
2447595.323018	2086716	3.5	2.0
2447596.311907	2087113	10.1	2.3
2447597.315602	2087516	4.8	1.7
2447598.319339	2087919	3.1	3.1
2447499.072036	2048072	6.5	3.2
2447532.768799	2061601	1.3	1.4
2447853.846325	2190511	4.3	2.1
2447856.832697	2191710	5.2	1.9
2447918.644630	2216527	2.6	3.1
2447920.619811	2217320	6.7	3.3
2447952.622834	2230169	-3.3	2.9
2447972.620899	2238198	9.6	6.1
2447973.709340	2238635	9.7	2.6
2447973.741682	2238648	6.5	1.4
2447978.770467	2240667	10.0	2.1
2447979.781717	2241073	11.8	3.1
2447980.319627	2241289	4.6	3.5
2447977.403038	2240118	7.5	2.3
2447978.327055	2240489	4.3	3.3
2447979.358189	2240903	2.6	3.4
2447979.358145	2240903	-1.2	4.9
2447978.601069	2240599	7.4	2.5
2447980.621017	2241410	5.8	3.4
2447980.782929	2241475	7.2	2.3
2447981.325918	2241693	8.4	1.4
2447981.592393	2241800	5.7	1.4
2447981.779185	2241875	4.8	1.1
2447982.329663	2242096	7.4	1.8
2447982.743093	2242262	5.0	1.2
2447983.734400	2242660	5.4	1.2
2447979.281057	2240872	9.5	2.9
2447980.224899	2241251	-2.4	2.9
2447984.735678	2243062	6.5	1.1
2448245.724666	2347847	-3.3	5.1
2448267.799932	2356710	5.2	2.3
2448324.627972	2379526	4.3	1.2
2448325.708938	2379960	4.1	1.3
2448328.593208	2381118	6.4	1.6
2448331.661735	2382350	4.0	1.2
2448238.571479	2344975	8.3	2.2
2448622.833258	2499253	3.3	1.8
2448680.642683	2522463	6.3	1.2
2448687.614155	2525262	4.0	1.2
2448688.597979	2525657	3.4	1.2
2449062.660365	2675840	4.2	1.6
2449063.609354	2676221	6.7	1.9
2449066.615640	2677428	6.5	1.4
2449066.371558	2677330	7.2	2.0
2449066.326737	2677312	8.2	2.6
2449069.342967	2678523	6.4	1.7
2449298.239287	2770423	8.5	4.1
2449298.304041	2770449	8.2	4.1
2449294.214264	2768807	5.5	4.1
2449294.293897	2768839	-0.5	4.1
2449295.439583	2769299	-4.0	6.1

Table 2
(Continued)

Time of Maximum BJDD	Epoch of Maximum	$O - C$ (s)	σ (s)
2449295.494387	2769321	-3.3	7.1
2449036.809260	2665461	2.4	2.2
2449038.677300	2666211	3.1	2.2
2449040.687310	2667018	3.6	4.1
2449041.616360	2667391	4.9	4.1
2449799.723888	2971765	5.6	1.3
2450427.920960	3223981	8.2	3.8
2450429.973242	3224805	2.7	2.4
2450430.914779	3225183	6.9	2.5
2450431.843821	3225556	7.5	1.5
2450434.912392	3226788	8.8	2.0
2450436.929828	3227598	5.4	1.7
2450483.633189	3246349	9.6	1.8
2451249.5989069	3553878	10.1	1.3
2451249.7632895	3553944	9.7	1.7
2451250.6126098	3554285	8.7	2.0
2451526.8772586	3665203	10.4	1.2
2451528.8523866	3665996	10.0	1.5
2451528.9196061	3666023	7.4	1.4
2451528.9868422	3666050	6.3	1.9
2451529.8585943	3666400	6.6	2.0
2451530.9097492	3666822	13.4	2.41
2451960.8561629	3839442	10.1	1.62
2451962.7864775	3840217	11.3	1.48
2451967.6806926	3842182	8.1	1.93
2451988.7919772	3850658	10.5	2.00
2451990.7845255	3851458	8.8	1.59
2452037.6472583	3870273	10.1	3.39
2452045.6399770	3873482	12.5	1.85
2452225.9050927	3945857	7.6	1.34
2452225.9598927	3945879	8.0	0.65
2452263.8834810	3961105	10.6	0.58
2452316.6442205	3980721	13.1	1.0
2452317.8995164	3982288	12.2	0.67
2452319.7999417	3982691	12.0	0.79
2452317.6479750	3982792	10.3	0.95
2452321.8348344	3983555	11.4	1.23
2452322.7265266	3984372	9.9	3.03
2452312.7412881	3984730	11.4	3.5
2452373.6840808	4089983	9.9	1.1
2452373.6839702	4090425	12.6	1.2
2452373.7140655	4090791	10.6	0.68
2452375.6392709	4122465	12.8	1.0
2452374.7700070	4124076	12.5	1.23
2452581.9494464	4134940	12.0	1.83
2452583.9095168	4137288	11.5	1.74
2452584.8812628	4144503	13.8	0.92
2452585.9821875	4148953	12.0	1.16
2452586.8937641	4146104	12.3	0.7
2452665.7845581	4255806	13.7	0.72
2452669.7970851	4256260	10.6	1.52
2452696.8561592	4257768	12.8	0.96
2452724.6624548	4267394	10.5	0.81
2453381.7442572	4409917	11.5	1.41
2453439.7653860	4433212	13.9	1.0
2453446.6073830	4435959	15.2	0.71
2453473.6191370	4446804	15.1	0.75
2453709.9576790	4541692	15.36	1.58
2453713.7883270	4543230	9.76	1.36
2453795.7202970	4576125	13.89	1.14
2453798.7440310	4577339	14.88	1.56
2453800.7291150	4578136	13.82	1.32
2454090.9940570	4694675	16.41	1.92
2454097.8708770	4697436	13.67	1.26

Table 2
(Continued)

Time of Maximum BJDD	Epoch of Maximum	$O - C$ (s)	σ (s)
2454175.7329770	4728697	13.56	2.10
2454505.6674710	4861163	16.64	1.09
2454536.7864160	4873657	17.32	1.16
2454538.7914220	4874462	15.95	1.21
2454539.5760330	4874777	19.16	1.43
2454860.8527290	5003767	14.62	1.18
2454861.8714540	5004176	16.72	1.16
2454865.7718960	5005742	15.80	1.43
2454935.2826668	5033650	17.80	2.00
2454937.3275356	5034471	17.34	2.67
2454945.716259	5037839	18.20	1.66
2455215.8113837	5146280	17.03	1.29
2455216.7429028	5146654	16.45	1.18
2455243.7347524	5157491	18.16	1.26
2455266.604463	5166673	18.74	1.76
2455272.6766822	5169111	17.25	1.83
2455273.588298	5169477	17.26	1.63
2455274.592065	5169880	19.53	1.42
2455276.6069443	5170689	15.42	3.27
2455542.8289250	5277575	19.59	1.28
2455567.8558979	5287623	18.64	1.48
2455570.8223324	5288814	18.49	1.33
2455593.7542828	5298021	17.52	1.29
2456395.6136513	5619961	19.00	1.44
2456405.6736629	5624000	21.75	1.16
2457039.68401488	5878550	21.05	4.19
2457040.73759366	5878973	21.76	1.79
2457095.73749568	5901055	24.57	1.27
2457097.63542361	5901817	25.14	0.96
2457100.62178721	5903016	25.28	0.62
2457101.62556613	5903419	27.23	14.81
2458189.71735867	6340279	27.19	1.32
2458190.59411461	6340631	29.42	1.41
2458191.66260081	6341060	26.95	1.22
2458192.59418283	6341434	31.81	1.50
2458192.68629503	6341471	28.00	2.65
2458146.67287842	6322997	25.35	0.79
2458145.70398597	6322608	24.83	0.58
2458144.72013874	6322213	23.40	0.85
2458488.81432050	6460364	26.35	0.54
2458870.45096380	6613588	27.75	3.14
2458902.63843304	6626511	29.26	13.8

where $\Delta E_0 = (T_{\max}^0 - T_{\max}^1)$, $\Delta P = (P - P_{=T_{\max}^0})$, and E is the epoch of the time of maximum T_{\max} , i.e., the integer number of cycles after our first observation T_{\max}^0 , which occurred in 1974 December 16.¹⁵

In Figure 1, we show the $O - C$ timings after subtracting the correction to period and epoch, and our best-fit curve through the data. The size of each point is proportional to its weight, i.e., inversely proportional to the square of uncertainty in phase. The error bars plotted are $\pm 1\sigma$. From our data through 2020, we obtain a new value for the epoch of maximum,

¹⁵ Fitting the whole light curve with a term proportional to $\sin\left[\frac{2\pi}{(P + \frac{1}{2}\dot{P})}t + \phi\right]$ by nonlinear least squares gives unreliable uncertainty estimates and the alias space in P and \dot{P} is extremely dense due to the 45 yr data set span (O'Donoghue 1994).

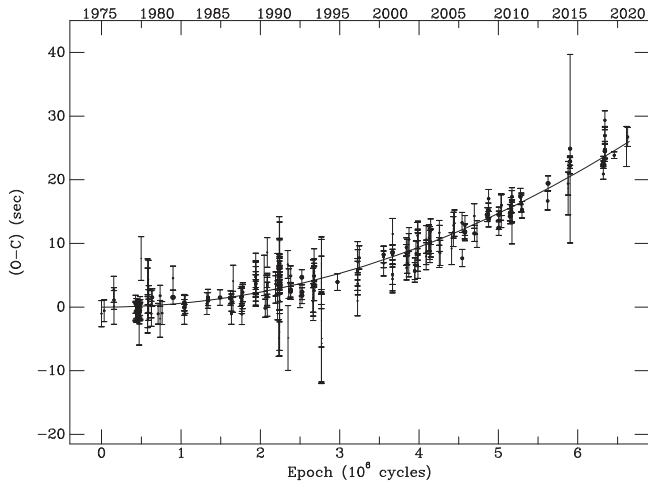


Figure 1. $(O - C)$: observed minus calculated times of maxima for the 215 s pulsation of G 117-B15A. The size of each point is proportional to its weight, i.e., inversely proportional to the uncertainty in the time of maxima squared. We show $\pm 1\sigma$ error bars for each point, and the line shows our best-fit parabola to the data. The fact that the line does not overlap these error bars is a demonstration that they are underestimated. Note that as the period of pulsation is 215.1973882 s, the observed total change in phase is only 50 deg.

$T_{\max}^0 = 244\,2397.9175141$ TCB ± 0.41 s, a new value for the period, $P = 215.19738823 \pm 0.00000063$ s, and most importantly, an observed rate of period change of:

$$\dot{P}_{\text{obs}} = (5.47 \pm 0.82) \times 10^{-15} \text{ s s}^{-1}.$$

Our quoted uncertainty is the most conservative estimate from the weighted average, which accounts for the reduction on the number of effective data points. For a comparison with the uncertainty published in Kepler et al. (2005), the internal uncertainty is now 0.32×10^{-15} , clearly underestimated from the changes in the value itself.

We use linear least squares to make our fit, with each point weighted inversely proportional to the uncertainty in the time of maxima for each individual run squared. We quadratically add an additional 1 s of uncertainty to the time of maxima for each night to account for external uncertainty caused perhaps by the beating of possible small amplitude pulsations (Kepler et al. 1995) or the small modulation seen in Figure 1. The amplitude, 1 s, is chosen as $4\langle A \rangle$ from the Fourier transform of the $O - C$. Such external uncertainty is consistent with Splaver et al. (2005) who show that the true uncertainties of the times of arrival of the millisecond pulsars are generally larger than the formal uncertainties, and that a quadratic term is added to them to fit the observations.

The satellite TESS observed G 115-B15A in Sector 21, almost continuously from 2020 January 21 to 2020 February 18. As the data is coadded on board to 120 s, and the camera is only 15 cm, the observed light curve resulted in an uncertainty of 13.8 s on the time of maximum of the 215 s pulsation. Even though the phase is in agreement with the observed $O - C$, it did not produce any improvement in our \dot{P} determination. Including the data from TESS, the values are unchanged, due to its large uncertainty. We note that TESS data in Sector 21 already includes the correction of 2 s to Data Product Timestamps in the pipeline,¹⁶ but there is still an extra uncertainty perhaps as large as 4 s in the TESS

timings, compared to ground observations (von Essen et al. 2020).

5. Discussion

We claim that the 215 s periodicity in G 117-B15A is the most stable optical clock known. According to Nicholson et al. (2015), their optical atomic clock based on 2000 ultracold strontium atoms trapped in a laser lattice lose no more than 1 s in 15 billion years, with an accuracy of $\dot{P} \leq 2 \times 10^{-18} \text{ s s}^{-1}$ in the JILA ^{87}Sr clock. Considering its period is 2.5×10^{-15} s, even though it is many orders of magnitude more accurate than G 117-B15A, it is less stable, as its timescale for period changes, i.e., the time it takes to lose a whole cycle, P/\dot{P} is 1250 s, compared to 1.2 Gyr for G 117-B15A. The total 26 s phase change observed for G 117-B15A after 45 yr of observations implies one cycle of the phase will be reached in 372.5 yr. In terms of accuracy, Brewer et al. (2019) reports the NIST $^{27}\text{Al}^+$ quantum-logic clock reached a systematic uncertainty of $\dot{P} \simeq 9.4 \times 10^{-19}$. Even the Hulse & Taylor's millisecond pulsar (Hulse & Taylor 1975), has a timescale for period change P/\dot{P} of only 0.35 Gyr (Damour & Taylor 1991), but the radio millisecond pulsar PSR J1909-3744 (Liu et al. 2020) has $\dot{P}_i = 2.60(3) \times 10^{-21} \text{ s s}^{-1}$, and a timescale of 18 Gyr, after 15 yr of observations. After correcting for the motion effects (pulsar proper motion, galactic differential acceleration, orbital motion, and general relativity correction), jitter, red, and white noise models. The timescale based on the spin of radio pulsars with millisecond periods can have a stability comparable to that of atomic timescales, but millisecond pulsars are also known to undergo sudden small glitch events (e.g., McKee et al. 2016), magnetospheric changes (Shannon et al. 2016), and effects relating to sudden changes in the interstellar medium (Lentati et al. 2016; Brook et al. 2018; Lam et al. 2018).

G 117-B15A was the first pulsating white dwarf to have its main pulsation mode index identified. The 215 s mode has $\ell = 1$, as determined by comparing the ultraviolet pulsation amplitude, measured with the Hubble Space Telescope, to the optical amplitude (Robinson et al. 1995). Using time-resolved spectra obtained at the Keck Telescope, Kotak et al. (2004) confirm the ℓ measurement for the $P = 215$ s pulsation and show that the other large amplitude modes, at 271 s and 304 s, show chromatic amplitude changes that do not fit simple single mode theoretical models (Robinson et al. 1995). Robinson et al. (1995) and Koester et al. (1994) derive T_{eff} near 12,400 K, while Bergeron et al. (1995, 2004) using a less efficient model for convection, estimated $T_{\text{eff}} = 11,630$ K. Gianninas et al. (2011) used $\text{ML2}/\alpha = 0.8$ models, which corrected to Tremblay et al. (2013) tri-dimensional convection calculations correspond to $T_{\text{eff}} = 12,420$ K, and $\log g = 8.12$. The uncertainty in effective temperature determinations from spectroscopy are of the order of 300 K and 0.05 dex in the surface gravity (Bergeron et al. 1995).

Benvenuto et al. (2002) show the seismological models with time-dependent element diffusion are only consistent with the spectroscopic data if the modes are $\ell = 1$, $k = 2, 3$, and 4, and deduces $\dot{M} = 0.525 M_{\odot}$, $\log(M_{\text{H}}/M_{\star}) \geq -3.83$ and $T_{\text{eff}} = 11\,800$ K, similar to those by Koester & Allard (2000). Their best model predicted a parallax $\Pi = 15.89$ mas, $\dot{P} = 4.43 \times 10^{-15} \text{ s s}^{-1}$, for the $P = 215$ s, $\dot{P} = 3.22 \times 10^{-15} \text{ s s}^{-1}$, for the $P = 271$ s, and $\dot{P} = 5.76 \times 10^{-15} \text{ s s}^{-1}$, for the $P = 304$ s periodicities.

¹⁶ https://archive.stsci.edu/missions/tess/doc/tess_drn/tess_reprocessing-sector_14_19_drn30_v02.pdf

Romero et al. (2012) used the mode identification and the observed periods of the three largest known pulsation modes to solve earlier degeneracy in solutions and derive a hydrogen layer mass best estimate of $1.25 \times 10^{-6} M_\star$, assuming $k = 2$ for the 215 s mode on their evolutionary C/O core white dwarfs, which resulted in $C/O = 0.28/0.70$ for its mass. The core composition is constrained mainly by the presence of the 304 s pulsation. In their Table 2, Córscico et al. (2012a) quote the theoretical rates of period change for the Romero et al. (2012) best-fit model as $\dot{P} = 1.25 \times 10^{-15}$, 4.43×10^{-15} , and 4.31×10^{-15} , for the $k = 2$, 3, and 4 modes. The $k = 2$ mode corresponds to the $P = 215$ s trapped mode in the hydrogen layer. Similar values were found by Bischoff-Kim et al. (2008) for their thicker hydrogen layer solution while their thinner solution had $\dot{P} \sim 3.0 \times 10^{-15}$. Córscico et al. (2012a) also show that because the $k = 2$ mode is trapped at the surface hydrogen layer, its rate of period change is almost insensitive to the core composition.

While it is true that the period change timescale can be proportional to the cooling timescale, it is also possible that other phenomena with shorter timescales can affect \dot{P} . The cooling timescale is the longest possible one.

As a corollary, if the observed \dot{P} is low enough to be consistent with evolution, then other processes, such as perhaps a magnetic field or diffusion induced changes in the boundary layers, are not present at a level sufficient to affect \dot{P} .

5.1. Theoretical Estimates and Corrections

5.1.1. Proper Motion

Stars are moving—they are observed to have a proper motion across the sky. As shown by Shklovskii (1970), and known as the “Shklovskii effect,” this means that the observed period derivatives will be higher than the intrinsic period derivative by an amount proportional to v^2/cd . Pajdosz (1995) estimated the influence of the proper motion of the star on the measured \dot{P} as:

$$\dot{P}_{\text{obs}} = \dot{P}_{\text{evol}}(1 + v_r/c) + P\dot{v}_r/c,$$

where v_r is the radial velocity of the star. Assuming $v_r/c \ll 1$ he derived

$$\dot{P}_{\text{pm}} = 2.430 \times 10^{-18} P(\text{s})(\mu[\text{''/yr}])^2 d(\text{pc}),$$

where \dot{P}_{pm} is the effect of the proper motion on the rate of period change, P is the pulsation period, μ is the proper motion, and d is the distance. The proper motion, $\mu = 0.1453 \pm 0.0001''/\text{yr}$, and the parallax, $\Pi = (0.01739 \pm 0.0008)''$, were estimated by Gaia DR2 (Gaia Collaboration et al. 2018), for both G 117-B15A and its proper motion companion G 117-B15B:

$$A: \pi = 17.386 \pm 0.080 \text{ mas} \quad d = 57.5 \pm 0.2 \text{ pc}$$

$$\mu = (-145.30 \pm 0.10, -0.006 \pm 0.088) \text{ mas yr}^{-1}$$

$$B: \pi = 17.437 \pm 0.101 \text{ mas}$$

$$\mu = (-145.99 \pm 0.12, -0.290 \pm 0.112) \text{ mas yr}^{-1}.$$

Therefore, $\dot{P}_{\text{pm}} = (0.3532 \pm 0.00024) \times 10^{-15} \text{ s s}^{-1}$, and the evolutionary—*intrinsic*—rate of period change \dot{P}_i :

$$\dot{P}_i = \dot{P}_{\text{observed}} - \dot{P}_{\text{pm}} = (5.12 \pm 0.82) \times 10^{-15} \text{ s s}^{-1}.$$

5.1.2. Limits on Mode Coherence

Montgomery et al. (2020) showed that the result of Hermes et al. (2017) that modes with periods longer than about 800 s are considerably less coherent than shorter period modes could be explained by their interaction with the time-dependent convection zone. Since the modes are assumed to acquire a small phase shift each time they reflect off the base of the convection zone, we can estimate the average amount of phase that would be accumulated by the 215 s mode over the total time base of observations. While the details are presented in Appendix A, we find that average accumulated phase would be only $\sim 4 \times 10^{-3}$ rad, which translates into a shift in the $O - C$ diagram of only ~ 0.13 s, i.e., negligible.

5.1.3. Effect of a Changing Magnetic Field

A weak magnetic field can perturb the oscillation frequencies of a star in much the same way that slow rotation does. If this magnetic field also slowly changes its magnitude with time, then it will produce a nonevolutionary \dot{P} for the modes. Here we provide an estimate of the size and rate of change of the magnetic field that would be required to mimic the observed \dot{P} for the 215 s mode; details are given in Appendix B.

Employing the same approach as Jones et al. (1989) and Montgomery (1994), we find that a uniform magnetic field that decreases from 280 to 0 G over a time period of 46 yr can produce $\dot{P} \approx 5.1 \times 10^{-15} \text{ s s}^{-1}$ for a 209 s, $k = 2$ mode. In addition, it is the change in B^2 that matters, so the same effect would be produced by a field that decreases from 2800 G over a period of 46 yr.

5.2. Pulsation Models

With time, as the temperature in the core of a white dwarf decreases, electron degeneracy increases and the pulsational spectrum of the star shifts to longer periods, in the absence of significant residual gravitational contraction. We compare the measured value of \dot{P}_i with the range of theoretical values derived from models with C/O cores subject to g -mode pulsations in the temperature range of G 117-B15A, which allow for mode trapping. Bischoff-Kim et al. (2008) estimated for their best model with $T_{\text{eff}} = 12656$ K, $M_\star = 0.602 M_\odot$, and a helium layer mass of $3.55 \times 10^{-3} M_\star$ $\dot{P} = (1.92 \pm 0.26) \times 10^{-15} \text{ s s}^{-1}$ if $\log(M_H/M_\star) = -6.2$ and $\dot{P} = (2.98 \pm 0, 17) \times 10^{-15} \text{ s s}^{-1}$ if $\log(M_H/M_\star) = -7.4$. The adiabatic pulsation calculations of Romero et al. (2012) with realistic evolutionary models, give a mass of $0.593 M_\odot$, $\log(M_H/M_\star) = 5.9$ and $\dot{P} \simeq 1.25 \times 10^{-15} \text{ s s}^{-1}$ for the $\ell = 1$, $k = 2$ observed oscillation.

The observed $P/\dot{P} = 1.33 \times 10^9$ yr is equivalent to 1 s change in period in 6.2 million years. We have therefore measured a rate consistent with the evolutionary timescale for this lukewarm white dwarf.

5.2.1. Core Composition

For a given mass and internal temperature distribution, theoretical models show that the rate of period change increases if the mean atomic weight of the core is increased, for models that have not yet crystallized in their interiors. As the evolutionary model cools, its core crystallizes due to Coulomb interactions between the ions (Lamb & van Horn 1975), and crystallization slows down the cooling by the release of latent

heat. Montgomery & Winget (1999) describe the effect of crystallization on the pulsations of white dwarf stars, but G 117-B15A is not cool or massive enough to have a crystallized core (Winget et al. 1997), or even for the convective coupling of the core to the envelope described by Fontaine et al. (2001) to occur.

The heavier the particles that compose the nucleus of the white dwarf, the faster it cools. The best estimate of mean atomic weight A of the core comes from the comparison of the observed \dot{P} with values from an evolutionary sequence of white dwarf models. Brassard et al. (1992) computed the rates of period changes for 800 evolutionary models with various masses, all with carbon cores but differing He/H surface layer masses, obtaining values similar to those of Winget et al. (1981), Wood & Winget (1988), and Bradley & Winget (1991). In those models, the average value of \dot{P} for all $\ell = 1, 2$, and 3 modes with periods around 215 s in models with an effective temperature around 13,000 K, and a mass of $0.5 M_{\odot}$, is $\dot{P}(\text{Ccore}) = (4.3 \pm 0.5) \times 10^{-15} \text{ s s}^{-1}$. Benvenuto et al. (2004) C/O models give $\dot{P}(\text{C/Ocore}) = (3 - 4) \times 10^{-15} \text{ s s}^{-1}$. Using a Mestel-like cooling law (Mestel 1952; Kawaler et al. 1986), i.e., $\dot{T} \propto A$, where A is the mean atomic weight in the core, one could write, for untrapped modes:

$$\dot{P}(A) = (3 - 4) \times 10^{-15} \frac{A}{14} \text{ s s}^{-1}.$$

All these models were computed assuming a thick $\log(M_{\text{H}}/M_{\star}) = 10^{-4}$ hydrogen layer, which lead to no significant mode trapping. The observed rate of period change is therefore consistent with a C or C/O core. The largest uncertainty comes from the models, essentially the hydrogen layer mass (Bischoff-Kim et al. 2008).

5.2.2. Reflex Motion

The presence of an orbital companion could contribute to the period change we have detected. When a star has an orbital companion, the variation of its line-of-sight position with time produces a variation in the time of arrival of the pulsation maxima, by changing the light travel time between the star and the observer by reflex motion of the white dwarf around the barycenter of the system. Kepler et al. (1991) estimated a contribution to \dot{P} caused by reflex orbital motion of the observed proper motion companion of G 117-B15A in their Equation (10) as:

$$\dot{P}_{\text{orbital}} = \frac{P_{\text{pul}}}{c} \frac{GM_B}{a_T^2} = 1.97 \times 10^{-11} P_{\text{pul}} \frac{M_B/M_{\odot}}{(a_T/\text{au})^2} \text{ s s}^{-1},$$

where a_T is the total separation, G here is the gravitational constant, and M_B is the mass of the companion star. In the above derivation they have also assumed the orbit to be nearly edge on to give the largest effect possible. G 117-B15A with Gaia magnitude $G = 15.5589 \pm 0.0010$, absolute magnitude $M_G = 11.760$, and Gaia color $G_{\text{BP}} - G_{\text{RP}} = -0.020$, Gaia DR2 parallax $\pi = (17.39 \pm 0.08)$ mas, proper motion $\text{ppm} = (145.34 \pm 0.10, -0.01 \pm 0.09)$ mas yr^{-1} , and its common proper motion companion G 117-B15B, with $G = 14.7270 \pm 0.0010$, $M_G = 10.934$, $\text{BP-RP} = 2.885$, $13.^{\circ}8$ away, $\pi = 17.43 \pm 0.10$ mas, $\text{ppm} = (-145.99 \pm 0.12, -0.29 \pm 0.11)$ mas yr^{-1} , are a common proper motion pair, forming a real binary system. Silvestri et al. (2002) measured the radial velocity

of G 117-B15B, assuming it formed a wide binary system with G 117-B15A as only $v_r = 2.2 \pm 9.4 \text{ km s}^{-1}$. Kotak et al. (2004) classifies G 117-B15B as an M3Ve from its spectra, obtained with the 10 m Keck I telescope, and measured $\log g \simeq 4.5$ and $T_{\text{eff}} \simeq 3400 \text{ K}$. Kirkpatrick et al. (2011) classifies G117-B15B as M3.5V from WISE colors. The mass of an M3.5V should be around $0.33 M_{\odot}$ (Lang 1999). With a separation of $13.^{\circ}8$, $a_T = 794 \text{ au}$, assuming the observed distance between G 117-B15A and B is at its largest ($\sin \omega \simeq 1$), where ω is the argument of periaxis. This corresponds to a lower limit on the orbital period of around 22 000 yr, and we estimate $\dot{P}_{\text{orbital}} \leq (1.1 \pm 1.1) \times 10^{-17} \text{ s s}^{-1}$. The large uncertainty takes into account the possibility the orbit might be strongly elliptical. Even though G 117-B15A and B form a real binary system, the contribution of the orbital reflex motion to the observed \dot{P} is negligible.

The whole observed phase change could also be caused by a planet of Jupiter's mass orbiting the white dwarf edge-on at a distance of 31 au, which corresponds to an orbital period around 314 yr, or a more massive planet in a less inclined orbit. Duncan & Lissauer (1998) show that such a planet would survive the post-main sequence mass loss. Any closer to the white dwarf, and such planets would produce a larger \dot{P} (e.g., Krzesinski et al. 2020). Note, however, that reflex motion produces sinusoidal variations on the $O - C$, which are distinguishable from parabolic variations after a significant portion of the orbit has been covered. This allows us to rule out the presence of planets as a function of orbital period and $M \sin i$, where i is the orbital inclination (see Figure 4 in Mullally et al. 2008). Considering a second-order derivative of the $O - C$ has not been detected yet, only planets with orbital periods longer than about 900 yr should be indistinguishable from a parabola, or if their effect on the $(O - C)$ is smaller than 1 s, i.e., with $M \sin i$ similar to the Earth's mass. The theoretical upper limit for a stable planetary orbit around G 117-B15A is around 0.3 a_T (Musielak et al. 2005), i.e., around 240 au, assuming the observed distance between G 117-B15A and B, a_T , is at its largest ($\sin \omega \simeq 1$), which would lead to a period of 4800 yr. At that distance, a planet would have to be more massive than $2.3 M_J$ to produce a phase change in 45 yr as large as the 26 s observed. Note that for half of the orbit the correction has the opposite sign. If the \dot{P} measured for other ZZ Cetis, like R548 (Mukadam et al. 2013) and L19-2 (Sullivan & Chote 2015) are also larger than the white dwarf cooling timescales, it is unlikely they are all caused by planets traveling away from us.

As discussed by Damour & Taylor (1991), any relative acceleration of the star with respect to the barycenter of the solar system will contribute to the observed \dot{P} . Their Equation (2.2) for the differential galactic orbits, decomposed in a planar contribution (2.12), where the second term is the proper motion correction, and a perpendicular contribution (2.28), applied to G 117-B15A, show the galactic contribution to be exactly the one calculated above for proper motion, i.e., the other terms are negligible—2–3 orders of magnitude smaller.

5.3. Axions

In Section 5.2 we list the predicted value of \dot{P} for the $k = 2$, $\ell = 1$ trapped mode for the evolutionary models as $\dot{P} \simeq 1.25 \times 10^{-15}$. As the value of the observed rate of period change is larger than the theoretical model, we study the

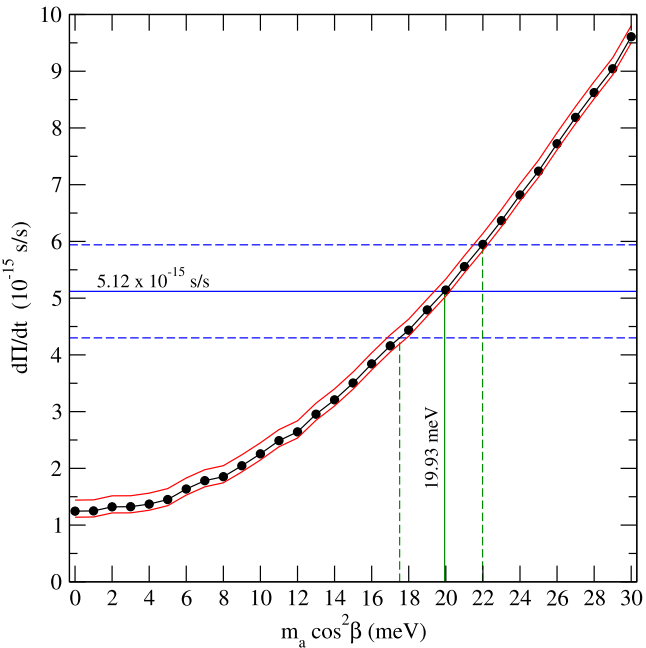


Figure 2. The rate of period change for the mode with $\ell = 1$ and $k = 2$, corresponding to a period of ~ 215 s in terms of the axion mass (black circles). Dashed lines represent the uncertainties in the value in the observed \dot{P} and the axion mass, while the red curves represent the internal uncertainties in \dot{P} due to modeling.

possibility of the excess of cooling as due to axions—hypothetical weakly interacting particles proposed as a solution to the strong charge-parity problem in quantum chromodynamics (Peccei & Quinn 1977). This possibility was first raised by Isern et al. (1992) since axions, similar to neutrinos, can escape carrying energy. At the time, employing semi-analytical models to the observed period change of G 117-B15A ($\dot{P} = 12 \pm 3.5 \times 10^{-15}$), they estimated a mass of $m_a \simeq 8.7$ meV. Kepler et al. (2000) published a value for \dot{P} ($2.3 \pm 1.4 \times 10^{-15}$), much lower than the previous value, and Córscico et al. (2001) estimated $m_a < 4.4$ meV using a detailed asteroseismological model. Later, with improved models and determination of \dot{P} (Kepler et al. 2005), Bischoff-Kim et al. (2008) estimated $m_a < 13.5$ meV. The determination of \dot{P} by Kepler (2012) was used by Córscico et al. (2012a) to estimate $m_a \simeq 17.4$ meV. This idea was also applied to other DAVs with \dot{P} known, finding $m_a \simeq 17.1$ meV for R 548 (Córscico et al. 2012b) and $m_a < 25$ meV for L 19-2 (Córscico et al. 2016).

Now, using the new determination for \dot{P} of G117-B15A we are able to set new constraints on the axion mass, assuming the extra cooling is due to the putative axion.

Using the value for the intrinsic \dot{P} , and assuming the effects from possible orbiting planets and magnetic fields are negligible, we estimate an axion mass using fully evolutionary models (see Figure 2) calculated with LPCODE (e.g., Althaus et al. 2010; Romero et al. 2012) including axions during all the white dwarf cooling. These results are very similar to those of Figure 5 of Córscico et al. (2012b). As a result we obtain a value of the coupling constant between axions and electrons $g_{ae} = (5.66 \pm 0.57) \times 10^{-13}$, or, adopting the DFSZ model (Zhitnitsky 1980; Dine et al. 1981), an axion mass $m_a \cos^2 \beta = 20 \pm 2$ meV. De Gerónimo et al. (2017) estimated the high and low limits for the $C(\alpha, \gamma) O$ reaction rate from the uncertainties given in Kunz et al. (2002). These limits are $0.55 \times$ and $1.1 \times$ factors in the reaction rate, which translates

into a central carbon abundance of $X_C = 0.450$ and $X_C = 0.246$ respectively, for the best-fit model for G 117-B15A. For the $k = 2$, $l = 1$ mode, corresponding to the 215 s mode, the value for \dot{P} , in the case where no axions are considered, changes by $\sim 15\%$ and $\sim 9\%$, respectively. Since this mode is trapped in the envelope, we do not expect large differences in the value of the rate of period change when the central composition changes (Córscico et al. 2016). Considering both the observational and model uncertainties, the estimated axion mass is $m_a \cos^2 \beta = 19.9_{-3.1}^{+2.1}$ meV.

6. Conclusions

We have measured the rate of change of the main pulsation period for the $T_{\text{eff}} \simeq 12,400$ K pulsating DA white dwarf G 117-B15A, the first ZZ Ceti to have its evolutionary rate of change measured, confirming it is the most stable optical clock known, with a rate of change of 1 s in $\simeq 6.2$ million years and a precise laboratory for physics at high energy. We note that mode trapping can reduce the rate of period change by up to a factor of 2 (Bradley 1996; Córscico et al. 2012a), but the changes in the trapping layers are still caused by cooling, and are included in our theoretical models.

After a large investment of telescope time to achieve such precision, we have measured the cooling rate of this 2.16 Gyr old white dwarf (Romero et al. 2012)—or 1.79 Gyr for our models with 20 meV axions. This estimate includes the time the star, with $M_{\text{initial}} \simeq 1.75 M_{\odot}$ (Romero et al. 2012), took to reach the white dwarf phase. We have also demonstrated it does not harbor planetary bodies similar to Jupiter in mass up to a distance around 30 au from the star, modulo $\sin i$, where i is the inclination to the line of sight. We cannot exclude larger distances or smaller planets with light travel time effects on the white dwarf smaller than 1 s.

This work was partially supported by grants from CNPq (Brazil), CAPES (Brazil), FAPERGS (Brazil) NSF (USA), NASA (USA). Z.P.V., D.E.W., and M.H.M. acknowledge support from the United States Department of Energy under grant DE-SC0010623, the National Science Foundation under grant AST 1707419, and the Wootton Center for Astrophysical Plasma Properties under the United States Department of Energy collaborative agreement DE-NA0003843. M.H.M. acknowledges support from the NASA ADAP program under grant 80NSSC20K0455. We acknowledge support through the TESS Guest Investigator Program Grant 80NSSC19K0378. K.J.B. is supported by the National Science Foundation under Award AST-1903828. This work has made use of data from the European Space Agency (ESA) mission Gaia (<https://www.cosmos.esa.int/gaia>), processed by the Gaia Data Processing and Analysis Consortium (DPAC, <https://www.cosmos.esa.int/web/gaia/dpac/consortium>). Funding for the DPAC has been provided by national institutions, in particular the institutions participating in the Gaia Multilateral Agreement. This paper includes data collected by the TESS mission. Funding for the TESS mission is provided by the NASA Explorer Program. We made extensive use of NASA Astrophysics Data System Bibliographic Service (ADS) and the SIMBAD and VizieR database, operated at CDS, Strasbourg, France.

Appendix A Estimate of Phase Drift of 215 s Mode

According to Montgomery et al. (2020), modes experience a small phase shift at their outer turning point due to the changing depth of the convection zone. If we assume that the average phase shift (due to the presence of multiple modes) is essentially random, then we can treat the accumulated phase after multiple reflections as a random walk. Denoting the average phase shift after one reflection as $\langle \Delta\phi \rangle$, then the average total phase shift after N cycles is given by

$$\langle \Delta\phi \rangle_{\text{tot}} = N^{1/2} \langle \Delta\phi \rangle. \quad (\text{A1})$$

Values of $\langle \Delta\phi \rangle$ can be obtained from the damping rate γ via the following relation (Equation (15) of Montgomery et al. 2020):

$$\gamma = \frac{1}{nP} \left(1 - \frac{\sin \langle \Delta\phi \rangle}{\langle \Delta\phi \rangle} \right) \approx \frac{1}{6nP} \langle \Delta\phi \rangle^2, \quad (\text{A2})$$

where n is the radial order of the mode and P is its period. Thus, we find that

$$\langle \Delta\phi \rangle_{\text{tot}} = (6n P \gamma N)^{1/2}. \quad (\text{A3})$$

For the relevant mode in G117-B15A, the total number of cycles is $N \approx 6 \times 10^6$, $n = 2$, $P \approx 215$ s, and, from Figure 9(a) of Montgomery et al. (2020), $\gamma < 10^{-15}$ s⁻¹ (and possibly much smaller than this), which yields a total phase shift of $\langle \Delta\phi \rangle_{\text{tot}} \approx 4 \times 10^{-3}$ rad. Thus, the average shift of the last point in the $O - C$ diagram should be $P \langle \Delta\phi \rangle_{\text{tot}} / 2\pi \approx 0.13$ s. Given this small value, the analysis of G117-B15A should be unaffected by the time-dependent effects of the surface convection zone.

Appendix B Effect of a Changing Magnetic Field

A pulsating white dwarf with a magnetic field should have its oscillation frequencies perturbed by the field. If that field changes with time (as has been directly observed in many astronomical objects) then the oscillation frequencies will also change with time.

For the case of oscillation frequencies perturbed by slow rotation, the use of perturbation theory is valid because the effects of rotation are small everywhere. This is not true for weak magnetic fields. Near the surface of a stellar model the gas pressure (P_{gas}) approaches zero while the magnetic pressure does not. Thus, there is always a region in which $B^2/8\pi > P_{\text{gas}}$, and, since the magnetic field geometry can modify the angular structure of the modes in this region, a self-consistent treatment can be quite complex (e.g., Dziembowski & Goode 1996; Bigot et al. 2000; Bigot & Dziembowski 2002).

Fortunately, we are only interested in the special case of the effect of a weak magnetic field on the frequencies of low-order g-modes in white dwarfs. These modes have outer turning points far below the region where $B^2/8\pi \sim P_{\text{gas}}$, so the perturbations to their frequencies do not strongly depend on their angular structure in the surface layers. Thus, a simple perturbative treatment as used in Jones et al. (1989) should be adequate for these modes.

Since we are only interested in order of magnitude estimates, we choose a constant field in the z direction aligned with the rotation axis. We also only consider the perturbation of $m = 0$

modes; the perturbation of other m values will be the same order of magnitude. Repeating the analysis in Montgomery (1994) for a “G117-B15A-like” model ($T_{\text{eff}} = 12,400$ K, $M_{\star} = 0.6M_{\odot}$), we find that a magnetic field that decreases in strength from 280 to 0 G over a time span of 46 yr can produce $\dot{P} \approx 5.1 \times 10^{-15}$ s s⁻¹ for a mode with $k = 2$ and $P = 209$ s. Furthermore, it is actually the change in B^2 that matters, i.e., ΔB^2 , so the same effect would be produced by a magnetic field that goes from 2814 to 2800 G over the same time span.

ORCID iDs

S. O. Kepler <https://orcid.org/0000-0002-7470-5703>
 D. E. Winget <https://orcid.org/0000-0003-0181-2521>
 Zachary P. Vanderbosch <https://orcid.org/0000-0002-0853-3464>
 J. J. Hermes <https://orcid.org/0000-0001-5941-2286>
 Keaton J. Bell <https://orcid.org/0000-0002-0656-032X>
 Alejandra D. Romero <https://orcid.org/0000-0002-0797-0507>
 M. H. Montgomery <https://orcid.org/0000-0002-6748-1748>
 Kurtis A. Williams <https://orcid.org/0000-0002-1413-7679>
 Staszek Zola <https://orcid.org/0000-0003-3609-382X>

References

Althaus, L. G., Córscico, A. H., Isern, J., et al. 2010, *A&ARv*, **18**, 471
 Benvenuto, O. G., Córscico, A. H., Althaus, L. G., & Serenelli, A. M. 2002, *MNRAS*, **332**, 399
 Benvenuto, O. G., García-Berro, E., & Isern, J. 2004, *PhRvD*, **69**, 082002
 Bergeron, P., Fontaine, G., Billéres, M., Boudreault, S., & Green, E. M. 2004, *ApJ*, **600**, 404
 Bergeron, P., Wesemael, F., Lamontagne, R., et al. 1995, *ApJ*, **449**, 258
 Biesiada, M., & Malec, B. 2002, *PhRvD*, **65**, 43008
 Bigot, L., & Dziembowski, W. A. 2002, *A&A*, **391**, 235
 Bigot, L., Provost, J., Berthomieu, G., et al. 2000, *A&A*, **356**, 218
 Bischoff-Kim, A., Montgomery, M. H., & Winget, D. E. 2008, *ApJ*, **675**, 1512
 Bradley, P. A. 1996, *ApJ*, **468**, 350
 Bradley, P. A., & Winget, D. E. 1991, *ApJS*, **75**, 463
 Brassard, P., Fontaine, G., Wesemael, F., & Tassoul, M. 1992, *ApJS*, **81**, 747
 Brewer, S. M., Chen, J.-S., Hankin, A. M., et al. 2019, *PhRvL*, **123**, 033201
 Brook, P. R., Karastergiou, A., McLaughlin, M. A., et al. 2018, *ApJ*, **868**, 122
 Castanheira, B. G., Kepler, S. O., Kleinman, S. J., et al. 2013, *MNRAS*, **430**, 50
 Córscico, A. H., Althaus, L. G., Miller Bertolami, M. M., et al. 2012a, *MNRAS*, **424**, 2792
 Córscico, A. H., Althaus, L. G., Miller Bertolami, M. M., et al. 2019, *A&ARv*, **27**, 7
 Córscico, A. H., Althaus, L. G., Romero, A. D., et al. 2012b, *JCAP*, **2012**, 010
 Córscico, A. H., Benvenuto, O. G., Althaus, L. G., Isern, J., & García-Berro, E. 2001, *NewA*, **5**, 197
 Córscico, A. H., Romero, A. D., Althaus, L. G., et al. 2016, *JCAP*, **2016**, 036
 Damour, T., & Taylor, J. H. 1991, *ApJ*, **366**, 501
 De Gérónimo, F. C., Althaus, L. G., Córscico, A. H., et al. 2017, *A&A*, **599**, A21
 Dine, M., Fischler, W., & Srednicki, M. 1981, *PhLB*, **104**, 199
 Duncan, M. J., & Lissauer, J. J. 1998, *Icar*, **134**, 303
 Dziembowski, W. A., & Goode, P. R. 1996, *ApJ*, **458**, 338
 Fontaine, G., & Brassard, P. 2008, *PASP*, **120**, 1043
 Fontaine, G., Brassard, P., & Bergeron, P. 2001, *PASP*, **113**, 409
 Gaia Collaboration, Brown, A. G. A., Vallenari, A., et al. 2018, *A&A*, **616**, A1
 Gianninas, A., Bergeron, P., & Ruiz, M. T. 2011, *ApJ*, **743**, 138
 Hermes, J. J., Gänsicke, B. T., Kawaler, S. D., et al. 2017, *ApJS*, **232**, 23
 Hulse, R. A., & Taylor, J. H. 1975, *ApJL*, **195**, L51
 Isern, J., García-Berro, E., Córscico, A. H., Benvenuto, O. G., & Althaus, L. G. 2004, *CoAst*, **145**, 13
 Isern, J., Hernanz, M., & García-Berro, E. 1992, *ApJL*, **392**, L23
 Jones, P. W., Hansen, C. J., Pesnell, W. D., & Kawaler, S. D. 1989, *ApJ*, **336**, 403
 Kawaler, S. D., Winget, D. E., Iben, I., & Hansen, C. J. 1986, *ApJ*, **302**, 530
 Kepler, S. O. 1993, *BaltA*, **2**, 515

Kepler, S. O. 2004, *IJMPD*, **13**, 1493

Kepler, S. O. 2012, in *ASP Conf. Ser.* 462, *Progress in Solar/Stellar Physics with Helio- and Asteroseismology*, ed. M. Shibahashi, M. Takata, & A. E. Lynas-Gray (San Francisco, CA: ASP), 322

Kepler, S. O., Costa, J. E. S., Castanheira, B. G., et al. 2005, *ApJ*, **634**, 1311

Kepler, S. O., Robinson, E. L., Nather, R. E., & McGraw, J. T. 1982, *ApJ*, **254**, 676

Kepler, S. O., Winget, D. E., Nather, R. E., et al. 1991, *ApJL*, **378**, L45

Kepler, S. O., Winget, D. E., Nather, R. E., et al. 1995, *BaltA*, **4**, 221

Kepler, S. O., Mukadam, A., Winget, D. E., et al. 2000, *ApJL*, **534**, L185

Kepler, S. O., Pelisoli, I., Koester, D., et al. 2019, *MNRAS*, **486**, 2169

Kepler, S. O. 1984, *ApJ*, **286**, 314

Kirkpatrick, J. D., Cushing, M. C., Gelino, C. R., et al. 2011, *ApJS*, **197**, 19

Koester, D. 2002, *A&ARv*, **11**, 33

Koester, D., & Allard, N. F. 2000, *BaltA*, **9**, 119

Koester, D., Allard, N. F., & Vauclair, G. 1994, *A&A*, **291**, L9

Kotak, R., van Kerkwijk, M. H., & Clemens, J. C. 2004, *A&A*, **413**, 301

Krzesinski, J., Blokesz, A., Siwak, M., & Stachowski, G. 2020, *A&A*, **642**, A105

Kunz, R., Fey, M., Jaeger, M., et al. 2002, *ApJ*, **567**, 643

Lam, M. T., Ellis, J. A., Grillo, G., et al. 2018, *ApJ*, **861**, 132

Lamb, D. Q., & van Horn, H. M. 1975, *ApJ*, **200**, 306

Lang, K. R. 1999, *Astrophysical Data: Planets and Stars* (New York: Springer)

Lauffer, G. R., Romero, A. D., & Kepler, S. O. 2018, *MNRAS*, **480**, 1547

Lentati, L., Shannon, R. M., Coles, W. A., et al. 2016, *MNRAS*, **458**, 2161

Liu, K., Guillemot, L., Istrate, A. G., et al. 2020, *MNRAS*, **499**, 2276

McGraw, J. T. 1979, *ApJ*, **229**, 203

McGraw, J. T., & Robinson, E. L. 1976, *ApJL*, **205**, L155

McKee, J. W., Janssen, G. H., Stappers, B. W., et al. 2016, *MNRAS*, **461**, 2809

Mestel, L. 1952, *MNRAS*, **112**, 583

Montgomery, M. H. 1994, MSc thesis, The Univ. Texas at Austin, <https://whitedwarf.org/theses/montgomery.pdf>

Montgomery, M. H., Hermes, J. J., Winget, D. E., Dunlap, B. H., & Bell, K. J. 2020, *ApJ*, **890**, 11

Montgomery, M. H., & Winget, D. E. 1999, *ApJ*, **526**, 976

Mukadam, A. S., Bischoff-Kim, A., Fraser, O., et al. 2013, *ApJ*, **771**, 17

Mullally, F., Thompson, S. E., Castanheira, B. G., et al. 2005, arXiv:astro-ph/0502520

Mullally, F., Winget, D. E., Degennaro, S., et al. 2008, *ApJ*, **676**, 573

Musielak, Z. E., Cuntz, M., Marshall, E. A., et al. 2005, *A&A*, **434**, 355

Nather, R. E., & Mukadam, A. S. 2004, *ApJ*, **605**, 846

Nather, R. E., Winget, D. E., Clemens, J. C., Hansen, C. J., & Hine, B. P. 1990, *ApJ*, **361**, 309

Nicholson, T. L., Campbell, S. L., Hutson, R. B., et al. 2015, *NatCo*, **6**, A6896

O'Donoghue, D. 1994, *MNRAS*, **270**, 222

Pajdusz, G. 1995, *A&A*, **295**, L17

Peccei, R. D., & Quinn, H. R. 1977, *PhRvD*, **16**, 1791

Robinson, E. L. 1979, in *Proc. IAU Coll.* 53, *White Dwarfs and Variable Degenerate Stars*, ed. H. M. Van Horn & V. Weidemann (Rochester: Univ. Rochester), 343

Robinson, E. L., Mailloux, T. M., Zhang, E., et al. 1995, *ApJ*, **438**, 908

Robinson, E. L., Kepler, S. O., & Nather, R. E. 1982, *ApJ*, **259**, 219

Romero, A. D., Córscico, A. H., Althaus, L. G., et al. 2012, *MNRAS*, **420**, 1462

Romero, A. D., Kepler, S. O., Córscico, A. H., et al. 2013, *ApJ*, **779**, 58

Shannon, R. M., Lentati, L. T., Kerr, M., et al. 2016, *ApJL*, **828**, L1

Shklovskii, I. S. 1970, *SvA*, **13**, 562

Silvestri, N. M., Oswalt, T. D., & Hawley, S. L. 2002, *AJ*, **124**, 1118

Smartt, S. J. 2009, *ARA&A*, **47**, 63

Splaver, E. M., Nice, D. J., Stairs, I. H., Lommen, A. N., & Backer, D. C. 2005, *ApJ*, **620**, 405

Standish, E. M. 1998, *A&A*, **336**, 381

Standish, E. M. 2004, *A&A*, **417**, 1165

Sullivan, D. J., & Chote, P. 2015, in *ASP Conf. Ser.* 493, 19th European Workshop on White Dwarfs, ed. P. Dufour, P. Bergeron, & G. Fontaine (San Francisco, CA: ASP), 199

Tremblay, P.-E., Ludwig, H.-G., Steffen, M., et al. 2013, *A&A*, **559**, A104

Vauclair, G. 2013, in *EAS Publ. Ser.* 63, *New Advances in Stellar Physics: From Microscopic to Macroscopic Processes*, ed. G. Alecian et al. (Les Ulis: EDP Sciences), 175

Vincent, O., Bergeron, P., & Lafrenière, D. 2020, *AJ*, **160**, 252

von Essen, C., Lund, M. N., Handberg, R., et al. 2020, *AJ*, **160**, 34

Winget, D. E., Hansen, C. J., & van Horn, H. M. 1983, *Natur*, **303**, 781

Winget, D. E., & Kepler, S. O. 2008, *ARA&A*, **46**, 157

Winget, D. E., Kepler, S. O., Kanaan, A., Montgomery, M. H., & Giovannini, O. 1997, *ApJL*, **487**, L191

Winget, D. E., van Horn, H. M., & Hansen, C. J. 1981, *ApJL*, **245**, L33

Wood, M. A., & Winget, D. E. 1988, in *Multimode Stellar Pulsations: Proceedings of the Workshop*, ed. G. Kovacs, L. Szabados, & B. Szeidl (Budapest: Konkoly Observatory), 199

Woosley, S. E., & Heger, A. 2015, in *Very Massive Stars in the Local Universe, Astrophysics and Space Science Library*, Vol. 412, ed. J. Vink (Cham: Springer), 199

Zhitnitsky, A. R. 1980, *SvJNP*, **31**, 260